

# Theory of high-order harmonic generation and attosecond pulse emission by a low-frequency elliptically polarized laser field

V. V. Strelkov\*

General Physics Institute of the Russian Academy of Sciences, Moscow, Russia  
and Centre Lasers Intenses et Applications, Université Bordeaux I, Talence, France

(Received 30 March 2006; published 19 July 2006)

We present a quantum-mechanical theory of xuv generation by an elliptically polarized intense laser field. Our approach is valid when the Keldysh parameter  $\gamma$  is about unity or less, and the driving ellipticity is less than  $\sqrt{2}\gamma$ . After the photoionization the motion of the electronic wave packet along the major axis of the driving field polarization ellipse is described quasiclassically, whereas the motion in the transverse direction is considered fully quantum mechanically; we also find the condition that allows the reduction of the motion description to a quantum orbit in the polarization plane of the laser field. We use the ionization rate calculated via numerical solution of the three-dimensional Schrödinger equation (TDSE), and take into account the Coulomb modification of the free electronic wave packet. The predictions of our theory for xuv emission agree well with numerical and experimental results. We study the high harmonic intensities and phases as functions of the driving intensity and ellipticity, and also the ellipticity and the rotation angle of the harmonic field polarization ellipse as functions of the driving ellipticity. The atomic response is decomposed into the contributions of different quantum paths. This allows finding a straightforward explanation for the observed dependencies.

DOI: [10.1103/PhysRevA.74.013405](https://doi.org/10.1103/PhysRevA.74.013405)

PACS number(s): 42.50.Hz, 32.80.Rm

## I. INTRODUCTION

High-order harmonic generation (HHG) accompanying photoionization of a gaseous medium by an intense laser field is finding more and more applications. The high harmonic radiation is used as a source for a time-resolved ultraviolet or soft x-ray spectroscopy. Nanolithography and nanoscopy are among the perspective applications. Besides, HHG makes possible a unique method for generation of xuv attosecond pulses ( $1 \text{ as} = 10^{-18} \text{ s}$ ), as it was first demonstrated experimentally in Ref. [1].

The HHG spectrum has typically a region of dozens or even hundreds of harmonics having comparable intensity ("plateau"), followed with a sudden decrease of the harmonic intensity ("cutoff"). A simple model of the phenomenon was suggested by Corkum [2] and by Kulander *et al.* [3,4]: at some time an electron is suddenly detached from the parent ion due to ionization and finds itself in a continuum with zero initial velocity; then it is accelerated with the laser field away from the parent ion; however, at the next half cycle of the laser field the electron is decelerated, driven back and, depending on the time of detachment, it can return to the parent ion and scatter off it [2]. The elastic scattering leads to the above threshold ionization (ATI), while the xuv is emitted due to the inelastic scattering. If the process occurs periodically (with a certain probability) every half cycle of the driving field, this xuv corresponds to the odd harmonics of the laser. This simple model correctly predicts the cut-off energy as a sum of the atomic ionization energy  $I$  and the

maximal kinetic energy which the electron can get during its free motion before scattering. Defining the latter energy from the classical analysis of the electron motion one finds the cut-off energy as  $I + 3.17U$  where  $U = E_0^2/4\omega_0^2$  is the ponderomotive energy (atomic units are used throughout the paper) for the laser field of an amplitude  $E_0$  and frequency  $\omega_0$ . Moreover, the model also explains the decrease of the HHG yield with the increase of the driving field ellipticity: the returning electron misses the ion when the laser field is (even slightly) elliptically polarized, and the emission is possible only due to the quantum mechanical spreading of the electronic wave packet. This model is often referred to as "simple-man model."

The quantum-mechanical models (more precisely, those where atom is described quantum mechanical whereas the field is still described classically) of the process in Refs. [5–8] were based on the strong-field approximation [9]. The case of elliptically polarized laser field was considered in Refs. [7,10,11]. This quantum-mechanical approach can be linked to the simple-man model via the application of the saddle point approximation to the integrals describing the atomic response to the driving field: the solutions of the equations for the saddle points (quantum paths) approximately correspond to the classical trajectories of the electron in the simple-man model. For every harmonic there are several contributions associated with different quantum paths from the initial bound state to the final state. Such paths, in analogy with classical orbits, are also called quantum orbits. The role of these paths for the HHG and ATI was first discussed in the early theoretical studies by Lewenstein *et al.* [6,12] and Becker *et al.* [7], and studied in details in Refs. [13–15] (also see Ref. [16] for a recent review). Strictly speaking, these quantum orbits are well defined in the tunneling limit which implies the following:

The laser field amplitude is much less than the atomic field  $E_a = (2I)^{3/2}$

---

\*Corresponding address: General Physics Institute of Russian Academy of Sciences, Theoretical Department, 38 Vavilova St., Moscow 119991, Russia; FAX: +7 495 135 0247. Email address: v-strelkov@fpl.gpi.ru

$$E_0 \ll E_a, \quad (1)$$

The laser photon energy is much less than the ionization energy

$$\omega_0 \ll I, \quad (2)$$

The Keldysh parameter is much less than unity:

$$\gamma \ll 1, \quad (3)$$

where the Keldysh parameter is

$$\gamma = \omega_0 \sqrt{2I/E_0} = \sqrt{I/2U}. \quad (4)$$

The validity of the quantum orbits approach for realistic laser parameters [which do not necessarily meet the requirement (3)] was investigated in the recent studies of Bauer *et al.* [17,18] via comparison with the results of the direct numerical TDSE solution.

Using the quantum orbits approach, Ivanov *et al.* [19] and Platonenko [20] suggested the HHG theories in which the atomic response amplitude was presented as a product of the terms responsible for ionization, free electronic wave-packet propagation, and the xuv emission. This decomposition allowed taking into account, at least approximately, the Coulomb corrections.

Note, that experimentally measured harmonic signal is determined not only by the atomic response, but also by the phase matching of the generation in the medium, propagation, and absorption of the xuv field. In this paper we concentrate on the single-atom properties of the xuv emission.

The HHG theory for the case of the elliptically polarized field has found an important application for studying single attopulse generation via polarization gating. This technique [21] relies on the strong HHG sensitivity to the driving ellipticity; using a laser pulse with time-varying ellipticity ensures the xuv emission only inside the “polarization gate” where the driving ellipticity is small. The signature of an isolated attosecond pulse generation with this method was demonstrated recently in Ref. [22] using a short laser pulse with a stabilized carrier-envelope phase.

In this paper (Sec. II) we present the theory of the xuv emission with elliptically polarized laser field. In contrast to other theories, we assume quasiclassical motion of the electron *only* in the direction of the major axis of the driving field polarization ellipse, whereas the electronic motion in the transverse direction is considered fully quantum mechanically. Such approach is motivated with the fact that the transverse motion is slow, and the range of validity of its quasiclassical description is, generally speaking, not evident *a priori*. We derive equations describing the atomic response for a limited (however, a sufficiently wide) range of driving ellipticities, and find conditions under which the transverse electronic motion can be considered quasiclassically as well. Besides, we take into account the Coulomb attraction of the wave packet right after the ionization (with a specific fitting parameter) and the Coulomb modification of the returning wave packet. Furthermore, we use the ionization rate calculated using direct numerical solution of the TDSE for a model atomic potential to determine both the ground state depletion and the population of the free wave packet.

Our theory is validated in Sec. III by comparison with the TDSE solution for linearly polarized driving field and also with published experimental data for the case of elliptically polarized field.

An important feature of our theory is that the contributions of the different quantum paths are separated within the frame of the single-atom response. In Sec. IV we study the properties of these contributions depending on the driving field parameters and find a rather straightforward explanation for some of these dependences within the quantum-orbit approach.

Finally, the results are discussed and an outline of the further studies is presented in Sec. V, and conclusions are made in Sec. VI.

## II. THEORY

We consider an atom in a single-electron approximation under the influence of the driving laser field; the instantaneous electric field strength and the vector potential are denoted as  $\mathbf{E}(t)$  and  $\mathbf{A}(t)$ , respectively, the magnetic component of the field is neglected. The field is either linearly polarized along the  $x$  axis or elliptically polarized in the  $x$ - $y$  plane and the major axis of the polarization ellipse is directed along the  $x$  axis.

The high-harmonic signal is determined by the second derivative of the atomic dipole moment. According to the Ehrenfest's theorem it is equal to the quantum-mechanical expectation value of the force acting on the electron

$$\ddot{\mathbf{d}}_{full}(t) = \mathbf{f}_{full}(t),$$

$$\mathbf{f}_{full}(t) = - \left\langle \Psi \left| \mathbf{E}(t) + \frac{\mathbf{r}}{r^3} \right| \Psi \right\rangle, \quad (5)$$

where  $\Psi$  denotes the time-dependent electronic wave function.

In the dipole approximation the first term in Eq. (5)

$$\langle \Psi | \mathbf{E}(t) | \Psi \rangle = \mathbf{E}(t) \langle \Psi | \Psi \rangle = \mathbf{E}(t)$$

evidently does not contain high-frequency oscillations. So below we consider the second term

$$\mathbf{f}(t) = - \left\langle \Psi \left| \frac{\mathbf{r}}{r^3} \right| \Psi \right\rangle. \quad (6)$$

We present the wave function as a sum of the bound state  $\varphi(r, t)$  and the free state  $\tilde{\chi}(\mathbf{r}, t)$

$$\Psi(\mathbf{r}, t) = \varphi(r, t) + \tilde{\chi}(\mathbf{r}, t). \quad (7)$$

Considering the bound state we take into account only the ground state (this approximation is usual for the HHG and ATI theories; its validity is discussed for instance in Refs. [6,8,11])

$$\varphi(r, t) = a(t) \varphi_0(r) \exp(iIt). \quad (8)$$

Here  $a(t)$  is the time-dependent bound state amplitude calculated as

$$a(t) = \left[ \exp \left( - \int_{-\infty}^t w(t') dt' \right) \right]^{1/2}. \quad (9)$$

The ionization rate  $w(t')$  is obtained via a direct numerical solution of the TDSE for a model atom as described in the next section.

In further studies we consider only free-bound transitions and neglect free-free transitions, as it was done in several theories of HHG [5–7,20]. Then, substituting Eq. (7) into Eq. (6) we have

$$\mathbf{f}(t) = - \left\langle \varphi(r, t) \left| \frac{\mathbf{r}}{r^3} \right| \tilde{\chi}(\mathbf{r}, t) \right\rangle + \text{c.c.} \quad (10)$$

Evidently, the operator  $\frac{\mathbf{r}}{r^3}$  is well localized near the nucleus. This allows us further (following Platonenko [20]) substituting the total continuum wave function  $\tilde{\chi}$  with its part that is close to the nucleus at the current time  $t$ . As it was discussed in the Introduction, this part, generally speaking, consists of several contributions (wave packets) associated with different quantum paths (or quantum orbits) returning to the origin at this time

$$\tilde{\chi}(\mathbf{r}, t) = \sum_m \chi^m(\mathbf{r}, t). \quad (11)$$

In the equations below the index  $m$  is omitted to shorten the notations; we will make the summation over  $m$  in the final equations.

Every wave packet  $\chi(\mathbf{r}, t)$  is expanded as

$$\chi(\mathbf{r}, t) = \int d^3p C(\mathbf{p}, t) \psi_{\mathbf{p}}(\mathbf{r}, t) \quad (12)$$

over the states

$$\psi_{\mathbf{p}}(\mathbf{r}, t) = \exp[-iS(\mathbf{p}, t) + iIt_i] \psi_{\mathbf{p}}^C(\mathbf{r}), \quad (13)$$

where

$$S(\mathbf{p}, t) = \int_{t_i}^t \frac{p^2(t')}{2} dt' \quad (14)$$

is the action calculated along the electron's trajectory starting at the origin at time  $t_i$  with some initial momentum, and finishing at  $x=0$  (and, generally speaking,  $y \neq 0$ ,  $z \neq 0$ ) at time  $t$  with mechanical momentum  $\mathbf{p}$ .

The term  $iIt_i$  in the phase of the wave function given by Eq. (13) provides the same phase of the bound and the free state at the instant of ionization  $t_i$ .

In Eq. (13)  $\psi_{\mathbf{p}}^C(\mathbf{r})$  is the continuum Coulomb state having momentum  $\mathbf{p}$  before scattering by the Coulomb potential. This state is written as (see Ref. [23])

$$\psi_{\mathbf{p}}^C(\mathbf{r}) = \exp\left(\frac{\pi}{2p}\right) \Gamma\left(1 - \frac{i}{p}\right) \exp(ipz') F\left(\frac{i}{p}, 1, ip(\rho' - z')\right), \quad (15)$$

where  $z' = \frac{\mathbf{p} \cdot \mathbf{r}}{p}$ ,  $\rho' = \sqrt{r^2 - z'^2}$  are coordinates of point  $\mathbf{r}$  in a cylindrical coordinate system whose axis is directed along vector  $\mathbf{p}$ ;  $F$  is a confluent hypergeometric function and  $\Gamma$  is gamma function.

Note that if a plane wave

$$\psi_{\mathbf{p}}^{\text{plane}}(\mathbf{r}) = \exp(i\mathbf{p} \cdot \mathbf{r}) \quad (16)$$

is used instead of the continuum Coulomb states (15) then Eqs. (12)–(14) present a standard expansion over the Volkov states. Later we will discuss the importance of using the continuum Coulomb states instead of the plane wave in this expansion.

Using the continuum Coulomb states (15) in Eqs. (12) and (13) can be explained as follows. The electron returns to the vicinity of the nucleus with momentum  $\mathbf{p}$  and then it is scattered by the Coulomb potential, but the electron's acceleration by the laser field during the collision time is small. Note that the latter is true at least for the harmonics in the upper part of the plateau because they are generated by wave packets returning to the origin when the instantaneous driving field is close to zero, so the field does not accelerate them. Thus, we are using the expansion over the Coulomb-Volkov states in the form close to those suggested in Refs. [24,25].

Substituting Eqs. (8), (12), and (13) into Eq. (10) we have

$$\mathbf{f}(t) = - \int d^3p a(t) C(\mathbf{p}, t) \left\langle \varphi_0(r) \left| \frac{\mathbf{r}}{r^3} \right| \psi_{\mathbf{p}}^C(\mathbf{r}) \right\rangle \times \exp[-iS(\mathbf{p}, t) - iI\tau] + \text{c.c.}, \quad (17)$$

where

$$\tau = t - t_i \quad (18)$$

is the time interval between the electron's detachment and return (travel time).

Consider the matrix element  $\langle \varphi_0(r) | \frac{\mathbf{r}}{r^3} | \psi_{\mathbf{p}}^C(\mathbf{r}) \rangle$  appearing in Eq. (17). This matrix element is a vector, and because of the spherical symmetry of the ground state wave function the direction of the vector is determined by the direction of the momentum  $\mathbf{p}$  of the free-state wave function. Due to the symmetry considerations (see Ref. [19] for more details) this matrix element can be presented as a product of the vector  $\mathbf{p}$  and a scalar that depends only on the absolute value of the momentum

$$\left\langle \varphi_0(r) \left| \frac{\mathbf{r}}{r^3} \right| \psi_{\mathbf{p}}^C(\mathbf{r}) \right\rangle = \mathbf{p} M^C(p). \quad (19)$$

Assuming that  $\varphi_0(r)$  is the 1s hydrogen state we calculate the matrix element  $M^C(p)$  numerically and then use its tabulated values. The matrix element as a function of  $p$  is shown in Fig. 1. We will discuss its behavior at the end of this section.

The important assumption of our approach is that the free motion of the electron along the  $x$  axis is considered quasiclassically. Another way of putting it is that we suppose that the motion in the  $x$  direction can be described in terms of quantum orbits. This assumption stems from the fact that the electron is strongly accelerated with the laser field in this direction because it is the direction of the main axis of the polarization ellipse; however, we do not assume that the motion in other directions is quasiclassical. As we discussed in the Introduction, the quasiclassic approach is valid in the tunneling limit; it is less applicable in the intermediate region between tunneling and multiphoton ionization regimes. In the next section we will compare the predictions of our

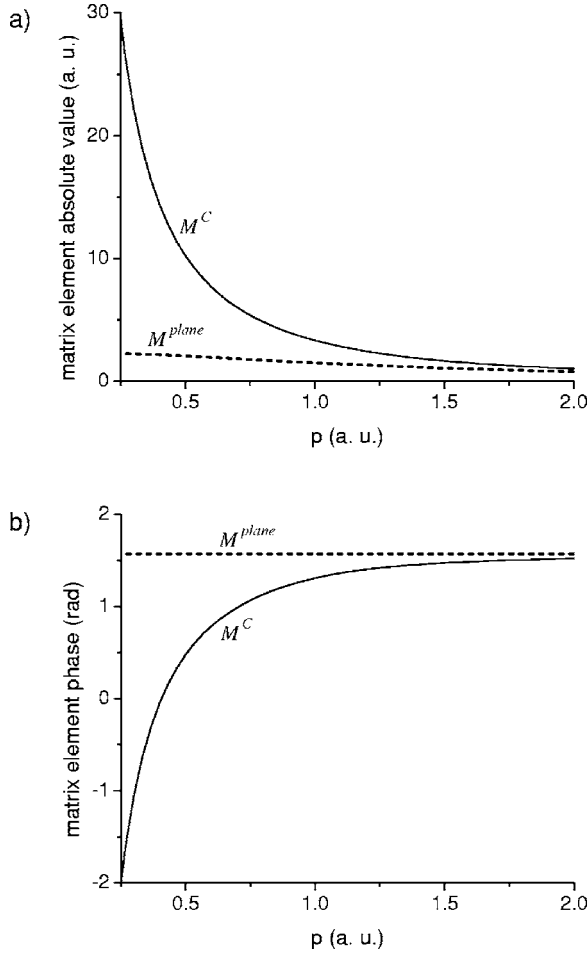


FIG. 1. Comparison of the matrix elements  $M^C(p)$  and  $M^{plane}(p)$  given by Eqs. (19) and (45), respectively. Graphs (a) and (b) show the absolute values and phases of the matrix elements. One can see that for the momentum values less than an atomic unit the role of the Coulomb attraction is non-negligible.

theory with the direct numerical results and discuss the validity of our approach for this region.

Thus, assuming that the electronic motion in the  $x$  direction is quasiclassic we consider in Eq. (17) only the value of the momentum  $p_x$  corresponding to the classical motion with zero initial momentum

$$\bar{p}_x(t) = \frac{1}{c}A_x(t) - \frac{1}{c}A_x(t_i), \quad (20)$$

so the momentum distribution in Eq. (17) is rewritten as

$$C(\mathbf{p}, t) = b(t, p_x) \delta(p_x - \bar{p}_x) C_{\perp}(p_y, p_z). \quad (21)$$

Substituting Eqs. (19), (21) in Eq. (17) we obtain

$$\begin{aligned} \mathbf{f}(t) = & - \int dp_y dp_z a(t) b(t, \bar{p}_x) C_{\perp}(p_y, p_z) \mathbf{p} M^C(p) \\ & \times \exp[-iS(\mathbf{p}, t) - iI\tau] + \text{c.c.} \end{aligned} \quad (22)$$

It is convenient to substitute in Eq. (22) the integration variable  $p_y$  with the following one:

$$\Delta p_y = p_y - \bar{p}_y, \quad (23)$$

where

$$\bar{p}_y(t) = \frac{1}{c}A_y(t) - \frac{1}{c}A_y(t_i) \quad (24)$$

is the  $y$  projection of the momentum of the classical electron with zero initial momentum. Thus,  $\Delta p_y$  is the initial momentum of the electron which returns to the origin having momentum  $p_y$ .

The distribution  $C_{\perp}(p_y, p_z)$  over the transverse momenta for the case of

$$\Delta p_y^2 + p_z^2 < 2I \quad (25)$$

was approximately found in Refs. [26,27]. In our notations it is written as

$$C_{\perp}(p_y, p_z) = \frac{\sqrt{2}}{\Delta p_{\perp} \sqrt{\pi}} \exp\left(-\frac{\Delta p_y^2 + p_z^2}{\Delta p_{\perp}^2}\right), \quad (26)$$

where  $\Delta p_{\perp}$  is the uncertainty of the transverse momentum of the electron after ionization. The value of this uncertainty was found analytically in Ref. [28]

$$\Delta p_{\perp}^2 = \frac{|E(t_i)|}{\sqrt{I/2}}. \quad (27)$$

Note that having in mind the approximate character of Eq. (27), we verified these results via the numerical TDSE solution (described in the next section). Namely, we studied the transverse spreading of the ionized wave-packet far from the origin and found that Eq. (27) describes this spreading very well.

The action  $S$  in Eq. (22) is given by Eq. (14). Using Eqs. (20) and (23) it is rewritten as

$$S = \frac{(\Delta p_y^2 + p_z^2)\tau}{2} + \Delta p_y \bar{y} + \bar{S}, \quad (28)$$

where

$$\bar{y} = \int_{t_i}^t \bar{p}_y(t') dt', \quad (29)$$

$$\bar{S} = \int_{t_i}^t \frac{\bar{p}_x^2(t') + \bar{p}_y^2(t')}{2} dt'. \quad (30)$$

The values  $\bar{y}$ ,  $\bar{S}$  can be understood as follows:  $\bar{y}$  is the  $y$  displacement at the instant of return to  $x=0$  of the electron started with zero initial momentum, and  $\bar{S}$  is the action calculated along its trajectory.

Finally, factor  $b(t, \bar{p}_x)$  in Eq. (22) can be found as it was done by Platonenko (see Eqs. (8), (14) in Ref. [20]). In our notations



$$b(t, \bar{p}_x) = a(t_i) \sqrt{\frac{w(t_i)}{\bar{p}_x} \frac{\partial t_i}{\partial t}}, \quad (31)$$

where  $w(t_i)$  is the ionization rate at the time of ionization,  $a(t_i)$  is the ground state amplitude [given by Eq. (9)] at this time.

Now, using Eqs. (23)–(31) we perform the integration in Eq. (22). The only approximation used here is that the matrix element  $M^C(p)$  is taken in stationary point of the integrand's phase; however, the matrix element  $M^C(p)$  is a slow-varying function (as can be seen from Fig. 1), so this approximation is well founded. After this the integration is performed exactly, without using the stationary phase method. Finally we obtain

$$\mathbf{f} = \sum_m \{f_x, f_y, 0\}, \quad (32)$$

$$f_x(t) = \sqrt{2\pi\bar{p}_x w(t_i) \frac{\partial t_i}{\partial t}} a(t_i) a(t) M^C \left[ \sqrt{\bar{p}_x^2 + \left(\bar{p}_y - \frac{\bar{y}}{\tau}\right)^2} \right] \times \frac{2i}{\Delta p_\perp \eta} \exp \left[ -i\bar{S} - iI\tau + \frac{i\bar{y}^2}{2\eta} \right] + \text{c.c.}, \quad (33)$$

$$f_y(t) = \sqrt{2\pi \frac{w(t_i)}{\bar{p}_x} \frac{\partial t_i}{\partial t}} \left[ \bar{p}_y - \frac{\bar{y}}{\eta} \right] \times a(t_i) a(t) M^C \left[ \sqrt{\bar{p}_x^2 + \left(\bar{p}_y - \frac{\bar{y}}{\tau}\right)^2} \right] \frac{2i}{\Delta p_\perp \eta} \times \exp \left[ -i\bar{S} - iI\tau + \frac{i\bar{y}^2}{2\eta} \right] + \text{c.c.}, \quad (34)$$

where

$$\eta = \tau - i \frac{2}{\Delta p_\perp^2}. \quad (35)$$

Equations (32)–(34) are the desired equations describing the single atom response as a function of time. Thus to calculate this response at a certain time  $t$  one should:

(i) Find all the ionization instants  $t_i^m$  leading to return at time  $t$ ; here we again [as in Eq. (11)] use the index  $m$  to number the ionization instants and the corresponding quantum paths which the electron could have followed to return at time  $t$  (note that the electron energies at the return time can differ for the different quantum paths). These ionization instants can be conveniently found with a graphical method suggested by Paulus *et al.* [29].

(ii) Calculate  $\bar{S}^m$ ,  $\bar{p}_x^m$ ,  $\bar{p}_y^m$ ,  $\bar{y}^m$ ,  $\partial t_i / \partial t$  for the  $m$ th quantum path.

(iii) Calculate  $f_x^m(t)$ ,  $f_y^m(t)$  with Eqs. (33), (34).

(iv) Summarize the contributions from different quantum paths [Eq. (32)].

Using the atomic response as a function of time one can calculate numerically the single atom spectrum as described in the end of this section.

Now let us discuss some features of the single-atom response given by Eqs. (33) and (34).

The factor  $a(t_i)a(t)$  in Eqs. (33) and (34) shows that xuv occurs if there is some ground state population at the time of ionization, *and also* at the time of return. In Ref. [30] we discuss this requirement in detail and confirm this conclusion by numerical results. Note that there is no such requirement in HHG theories suggested in Refs. [6,7], because they consider slow variation of the ground state population, thus the difference in populations at the instants of ionization and return is supposed to be negligible.

Equations (33) and (34) can be simplified when

$$\tau \gg 2/\Delta p_\perp^2. \quad (36)$$

Introducing the transverse size of the wave packet at the time of return

$$\rho^2 = 4/\Delta p_\perp^2 + \Delta p_\perp^2 \tau^2, \quad (37)$$

we see that inequality (36) means that the travel time is long enough, so that due to the wave packet spreading its transverse size is much larger than the initial transverse size. If the condition (36) is satisfied, then Eqs. (33) and (34) can be rewritten as

$$f_x(t) = \sqrt{2\pi\bar{p}_x w(t_i) \frac{\partial t_i}{\partial t}} a(t_i) a(t) M^C \left[ \sqrt{\bar{p}_x^2 + \left(\bar{p}_y - \frac{\bar{y}}{\tau}\right)^2} \right] \frac{2i}{\rho} \times \exp \left[ -iS_{\text{quasi-cl.}} - iI\tau - \frac{\bar{y}^2}{\rho^2} \right] + \text{c.c.}, \quad (38)$$

$$f_y(t) = \sqrt{2\pi \frac{w(t_i)}{\bar{p}_x} \frac{\partial t_i}{\partial t}} \left[ \bar{p}_y - \frac{\bar{y}}{\tau} \right] \times a(t_i) a(t) M^C \left[ \sqrt{\bar{p}_x^2 + \left(\bar{p}_y - \frac{\bar{y}}{\tau}\right)^2} \right] \frac{2i}{\rho} \times \exp \left[ -iS_{\text{quasi-cl.}} - iI\tau - \frac{\bar{y}^2}{\rho^2} \right] + \text{c.c.}, \quad (39)$$

where

$$S_{\text{quasi-cl.}} = \int_{t_i}^t \frac{\bar{p}_x^2(t') + \left(\bar{p}_y(t') - \frac{\bar{y}}{\tau}\right)^2}{2} dt' \quad (40)$$

is the action calculated along the trajectory starting with the initial y momentum  $\Delta p_y = -\bar{y}/\tau$  and therefore returning to the origin. Thus under the condition (36) the electronic motion can be reduced to the quantum orbit lying in the  $x$ - $y$  plane, i.e., motion both in  $x$  and  $y$  directions can be considered quasi-classically. Note also that the factors  $1/\rho$  and  $\exp[-\frac{\bar{y}^2}{\rho^2}]$  in Eqs. (38) and (39) describe the decrease of the xuv emission due to the wave packet spreading and its  $y$  drift in the elliptically polarized field, respectively.

Using Eq. (27), the inequality (36) can be rewritten as

$$\tau \gg \frac{\sqrt{2I}}{|E(t_i)|}. \quad (41)$$

This inequality is satisfied in the tunneling limit. Thus Eqs. (38)–(40) can be used, for instance, to describe xuv generation with several micron driving wavelength, studied re-

cently in Refs. [31–33]. However, for more typical driving field parameters (the Ti:Sapp laser wavelength and the intensity of units of  $10^{14}$  W/cm<sup>2</sup>) the inequality (41) is hardly valid for the shortest quantum path. In the latter case the validity of the quasiclassical description for the motion in  $y$  direction is questionable, and Eqs. (33) and (34) should rather be used.

Now we will discuss the highest driving ellipticity that leaves our approach still applicable. The key limitation for the ellipticity follows from using the distribution (26) over the transverse momenta, which is valid if the inequality (25) is satisfied. As can be seen from Eqs. (1) and (27), this inequality is satisfied for the bulk of the wave packet; for the high momenta [where the inequality (25) is not satisfied] the wave function amplitude is very low (the distribution valid for such transverse momenta can be found in Refs. [26,27,34]). If the main contribution to the integral (22) comes from these momenta, then xuv emission is weak. Thus, our approach is valid up to ellipticities for which the generation is sufficiently suppressed, i.e., up to ellipticities essentially exceeding the threshold ellipticity  $\varepsilon_{th}$ . ( $\varepsilon_{th}$  is the driving ellipticity that causes a decrease by a factor of 2 in harmonic intensity compared to the case of linear driving polarization.)

The typical energy of the transverse electronic motion is about  $\varepsilon^2 U$ , so the requirement (25) can be rewritten as

$$\varepsilon^2 U < I. \quad (42)$$

Using the Keldysh parameter given by Eq. (4) we obtain the desired validity range

$$\varepsilon < \sqrt{2}\gamma. \quad (43)$$

Finally, let us discuss the role of the Coulomb attraction. Let us substitute a plane wave (16) instead of the continuum Coulomb function (15) into Eq. (13). Then instead of the matrix element (19) we have the matrix element

$$\left\langle \varphi_0(r) \left| \frac{\mathbf{r}}{r^3} \right| \psi_p^{plane}(\mathbf{r}) \right\rangle = \mathbf{p} M^{plane}(p). \quad (44)$$

For  $\varphi_0(r)$  equal to  $1s$  hydrogen state this matrix element can be calculated analytically

$$M^{plane}(p) = \frac{4\sqrt{\pi}i}{p^3} [p - \arctan(p)]. \quad (45)$$

The matrix elements  $M^{plane}(p)$  and  $M^C(p)$  are compared in Fig. 1. One can see that they are close to each other for high values of the momentum, and differ much for the momenta less than unity. Thus the role of the Coulomb modification of the returning wave packet is essential for the harmonics with photon energy about two ionization energies and less.

In the next sections we study intensities and phases of the spectral components of  $x$  and  $y$  projections of the atomic response. The spectrum of the single-atom response is found as follows. We divide the time interval where the atomic response is nonzero (usually this time interval coincides with the one where the laser pulse envelope is nonzero) into short time steps; the step duration is chosen to be much less than

the period of the highest-frequency xuv that can be emitted (the latter can be estimated using the  $I+3U$  law). The atomic response as a function of time is found at this temporal grid using Eqs. (32)–(34). Then we calculate the spectrum, making numerically the integration

$$f_{x,y}(\omega) = \frac{1}{2\pi} \int f_{x,y}(t) \exp(i\omega t) dt, \quad (46)$$

over the time interval where the atomic response is nonzero.

Note, that in our approach it is not supposed that the laser pulse is quasimonochromatic [we used directly the electric field strength  $\mathbf{E}(t)$  and the vector potential  $\mathbf{A}(t)$  as functions of time]. This allows, in particular, studying the xuv generation with short, even few-cycle, laser pulses. Moreover, our approach is applicable when the  $x$  and  $y$  components of the laser field vary with time in different ways, leading to the field with time-varying ellipticity.

The intensity of the xuv attosecond pulse is calculated as

$$J_{XUV}(t) = \left| \int_{\Omega_{low}}^{\Omega_{up}} f_x(\omega) \exp(-i\omega t) d\omega \right|^2 + \left| \int_{\Omega_{low}}^{\Omega_{up}} f_y(\omega) \exp(-i\omega t) d\omega \right|^2, \quad (47)$$

where  $\Omega_{low}$  and  $\Omega_{up}$  are the lower and the upper edge of the frequency range used to obtain the attopulses.

### III. NUMERICAL TDSE SOLUTION

To find the fitting parameters for our theoretical approach and to test it we solve numerically the TDSE for a single-electron atom with a model potential reproducing Ar atom. Our approach for the TDSE solution is presented in Ref. [30] and the model atomic potential is described in Ref. [35].

Using the numerical solution of the TDSE we find the ionization rate for the atom in a (quasi-) static electric field as a function of the field strength. This is done with a method used by Bauer and Mulser [36]. Note that the found ionization rates are very close to those we used in Refs. [37–40]. The latter were calculated via another approach: the TDSE was solved numerically with a  $B$ -spline method described in Ref. [41] for a model argon potential suggested by Muller [42].

Then we calculate the ionization rate at time  $t_i$  as the static-field ionization rate for the field strength at a slightly earlier time

$$w(t_i) = w\{[E(t_i - \delta)]\}. \quad (48)$$

The retardation time  $\delta$  describes roughly the noninstantaneity of the ionization and attraction of the ionized electron to the parent ion after the ionization. The value of  $\delta$  is chosen to reach better agreement of the numerical and theoretical results on the xuv generation with laser field. The best fit was achieved for  $\delta=1$  atomic unit; this value is used in all the calculations below.

Note that the static-field ionization rate was used in HHG theories [19,20]. However, in both papers analytical equations for ionization rate were utilized. This is less accurate

than using the tabulated ionization rate suggested in this paper (the study of accuracy of different analytical equations for ionization of hydrogen can be found in Ref. [36]). Using the retardation in the instantaneous ionization rate calculation was suggested by Platonenko [20].

Using the numerical TDSE solution in a static electric field we also verified the result (27) studying the transverse spreading of the ionized wave-packet far from the origin. We found very good agreement between predictions of Eq. (27) and the numerical results.

Below we compare theoretical and numerical results on the xuv generation by laser field. We use the driving field in the following form:

$$\tilde{A}_0(t) = \begin{cases} A_0 \sin^2\left(\frac{\pi t}{2\tau_{front}}\right), & 0 < t \leq \tau_{front} \\ A_0, & \tau_{front} < t \leq \tau_{front} + \tau_{top} \\ A_0 \sin^2\left(\frac{\pi(t - [\tau_{front} + \tau_{top}])}{2\tau_{front}}\right), & \tau_{front} + \tau_{top} < t \leq 2\tau_{front} + \tau_{top} \\ 0, & \text{otherwise.} \end{cases} \quad (52)$$

Note that the field given by Eqs. (51) and (52) satisfies the condition

$$\int_{-\infty}^{\infty} E_{x,y}(t) dt = 0. \quad (53)$$

This condition means the absence of a static component of the field and thus should be satisfied for any laser field (see [43] and references therein).

Using the amplitude of the vector potential  $A_0$  and the laser frequency  $\omega_0$  we define the amplitude of the electric field  $E_0 = \omega_0 A_0 / c$ , the laser peak intensity  $J = cE_0^2 / 8\pi$ , the ponderomotive energy  $U = E_0^2 / 4\omega_0^2$  and the laser cycle duration  $T = 2\pi / \omega_0$ .

Much effort has been put recently into the studies of attopulse generation using a group of high harmonics (see, for example [1,22,44–46]). This leads to a conclusion that the correct prediction of the properties of xuv emission on the attosecond scale is very important. So comparing our theory with the numerical results we focus on attopulse generation. The attosecond pulses are calculated by Eq. (47) utilizing theoretical and numerical spectrum. We use the laser pulse described by Eqs. (49)–(52) with  $\tau_{front} = \tau_{top} = T$  linearly polarized in the  $x$  direction with  $\phi = 0$ . Evidently, only  $x$  projection of the atomic response is nonzero. The theoretical results are obtained taking into account only two quantum paths corresponding to the travel time  $\tau$  less than one fundamental cycle (these quantum paths were numbered 1, 2 in Refs. [14,47]). Following Refs. [37–39] we denote the contributions to the harmonic from the shorter and the longer paths as SP and LP, respectively. The contributions of quan-

$$A_x(t) = \tilde{A}_0(t) \sin(\omega_0 t + \phi), \quad (49)$$

$$A_y(t) = \varepsilon \tilde{A}_0(t) \cos(\omega_0 t + \phi), \quad (50)$$

$$E_{x,y} = -\frac{1}{c} \cdot dA_{x,y}/dt. \quad (51)$$

Here  $\tilde{A}_0(t)$  is the envelope of the vector potential,  $\varepsilon$  is the laser field ellipticity,  $\phi$  is the carrier-envelope phase. We use the “flat-top” envelope which rises during time interval  $\tau_{front}$ , then it is constant during time interval  $\tau_{top}$ , and finally it falls during time interval  $\tau_{front}$ .

tum paths with  $\tau > T$  are lower because of the spreading of the electron wave-packet in the transverse direction [6]; moreover, for such short laser pulse these contributions are negligible. The results for different peak driving intensities are shown in Figs. 2 and 3. Two attopulses are emitted per the fundamental half cycle when the used harmonic group is within the plateau. These attopulses can be attributed to the contributions of the shorter and longer quantum path [47,48]. In Fig. 2 one can see, in particular, that our theory correctly predicts the ratio of these contributions. The duration of the attopulses and the time of the emission also agree with the numerical results.

Thus, from Fig. 2 one can conclude that there is a good quantitative agreement between the theory and numerical calculation for the Ti:Sapphire laser driving field with intensity of several units of  $10^{14}$  W/cm<sup>2</sup> ( $\gamma \approx 1$ ). This agreement proves the applicability of the approximations used in our theory under these (rather typical for HHG) conditions.

Unfortunately, numerical solution of the TDSE for elliptically-polarized laser field requires much more laborious computations than those for the linearly-polarized field. So the comparison of the theory with the direct numerical results for the nonzero ellipticity is currently unavailable for us.

#### IV. RESULTS

In this section we present some results of calculations of high harmonic properties using our theory. However, the detailed study of the harmonic generation and attopulse emis-

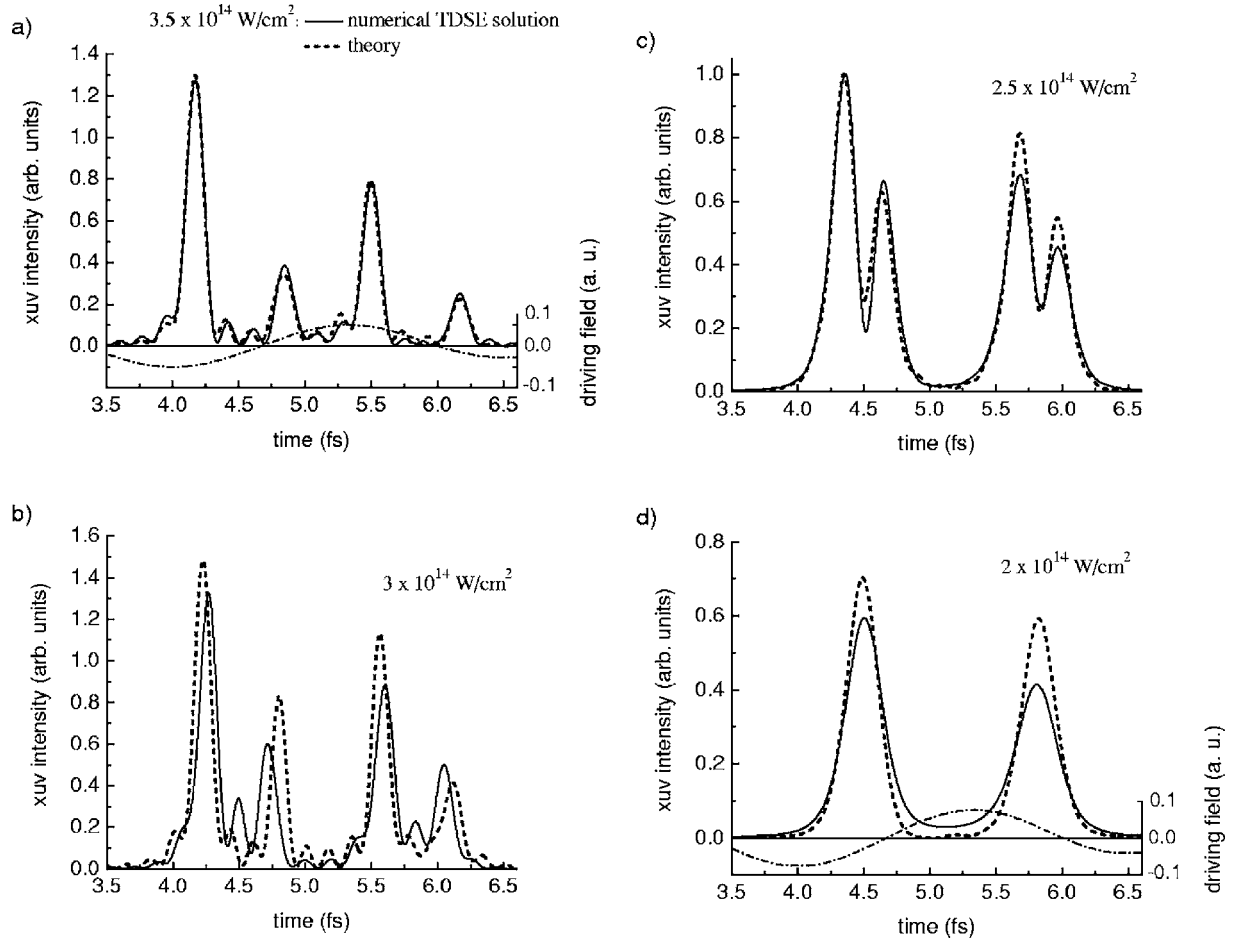


FIG. 2. The xuv intensities calculated with Eq. (47) using the spectra obtained theoretically (dashed line) and numerically via the TDSE solution (solid line) for a model Argon potential. The frequency range used in Eq. (47) is from  $\Omega_{low}=50$  eV (approximately  $32\hbar\omega_0$ ) to  $\Omega_{up}=75$  eV (approximately  $48\hbar\omega_0$ ), the ionization energy is  $I=15.75$  eV (Argon), the driving pulse is linearly polarized, the wave length is  $0.8 \mu\text{m}$ , the peak intensities are shown in the graphs; they correspond to the formal cut-off  $q_{max}=(I+3.17U)/\hbar\omega_0$  at approx. 53rd (a), 47th (b), 41st (c), and 35th (d) harmonic. The theoretical and numerical xuv intensities for all the four graphs are normalized using the intensity of the first peak in the graph (c). A good agreement of the theory with the numerical results for different driving intensities can be seen.

sion with our theory is far above the scope of this paper. So, we restrict ourselves here with relatively low driving field ellipticities; the case of such ellipticities is of practical importance because the harmonic signal rapidly decreases with the driving ellipticity. We discuss here only the contributions of the quantum paths with the travel time less than one fundamental cycle. For the low driving ellipticities these contributions are more important than those corresponding to times of flight exceeding fundamental cycle (however, this is not the case for higher driving ellipticities [49]). Moreover, we consider here only the laser field whose ellipticity is constant in time. Note that, as we have already mentioned in the end of Sec. II, our approach allows studying the case of time-varying ellipticity as well; in Refs. [22,37–40] we applied the theory to study single attopulse generation via ellipticity gating.

To study harmonic properties we use the fundamental pulse with  $\tau_{front}=T$  and  $\tau_{top}=10T$ . Using such long flat-top pulse makes interpretation of the theoretical results easier. In particular, the harmonic lines are very sharp because there is almost no broadening of the lines due to the dependence of

the harmonic phase on the fundamental intensity. Absence of the broadening makes definition of the calculated harmonic phase easier.

In Figs. 4 and 5 we show intensities and phases of the 17th and 21st harmonics as functions of the laser peak intensity. The results for the contribution of the shorter and longer trajectories are presented separately. One can see in the Figs. 4(a) and 5(a) (as well as in Fig. 3) that the contributions of the two quantum paths, in general, are comparable. This conclusion agrees with the results of the numerical calculations [20,50–52]. Thus our theory predicts more realistic amplitudes of the quantum path contributions than the Lewenstein's theory [6], which (as it was stressed by Gaarde and Schafer [52]) often overestimates the contribution of the longer quantum path.

One can see that the intensities of the two contributions for the 21st harmonic are closer to each other than those for the 17th harmonic. This is natural because the 21st harmonic is closer to the cutoff where the both contributions merge with each other. Also in the Figs. 4(a) and 5(a) we can see that the harmonic signal stops growing with the intensity and



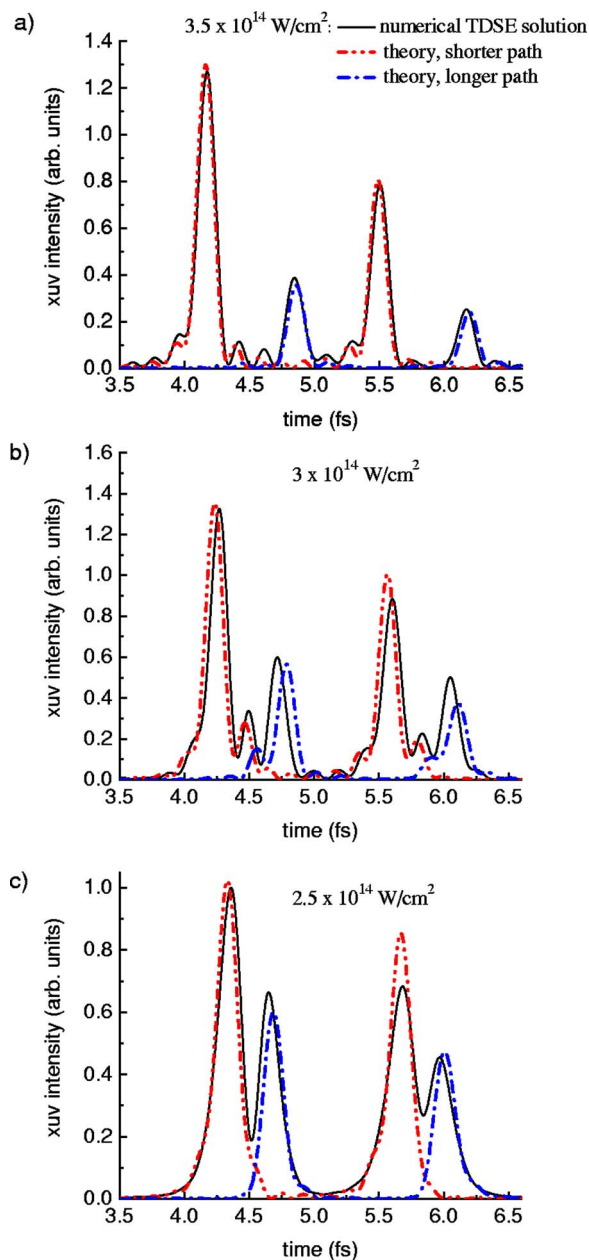


FIG. 3. (Color online). The same as Fig. 2, but the contributions from the two quantum paths corresponding to the travel time less than one fundamental cycle are given separately: the dot-dot-dashed (red online) line shows the contribution from the shorter path (SP) and the dot-dashed (blue online) line shows the contribution from the longer one (LP). Two attopulses per one fundamental half cycle are predicted by the numerical simulation, which can be attributed to the two quantum path. When the harmonic group is totally within the plateau [graph (a)] the attopulses are well separated, whereas they partly superimpose and interfere when the harmonic group includes the cut-off region [graphs (b), (c)]. Finally, the two contributions can not be separated if the group is totally in the cut-off region [see Fig. 2(d)].

then decreases. This feature was studied numerically in details in our recent paper [30].

When the harmonics are within the plateau region the phases of both contributions depend almost linearly on the

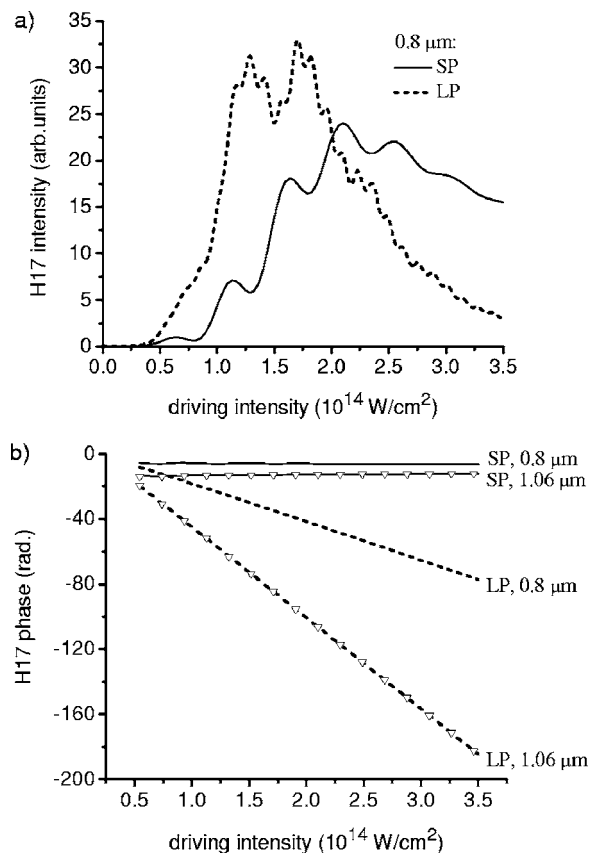


FIG. 4. The 17th harmonic intensity (a) and phase (b) as a function of the driving intensity. The contributions of the shorter and the longer quantum paths are shown with solid and dashed lines, respectively. The driving radiation is linearly polarized; its wavelength is 0.8  $\mu\text{m}$  for both curves in graph (a), 0.8  $\mu\text{m}$ , and 1.06  $\mu\text{m}$  (see legend) for graph (b).

driving intensity [see Figs. 4(b) and 5(b)], in agreement with the numerical results presented in Refs. [50,51]. The behavior of the phases of the contributions is very similar for the 21st and the 17th harmonic. For the lower driving frequency the phase dependence on the driving intensity is stronger. Namely, the slopes of the lines in Figs. 4(b) and 5(b) are proportional to  $1/\omega_0^3$ .

In our earlier publication [37] we have shown that our theory reproduces quite well the decrease of the 21st harmonic intensity with the driving ellipticity increase measured experimentally in Refs. [53,54]. In Fig. 6 we show the calculated threshold ellipticities for different harmonics and compare them with the recent experimental results [22]. The theoretical results are shown separately for the shorter and the longer path component. A reasonable agreement is found for all harmonics. However, experimentally the threshold ellipticity is lower. The discrepancy can be explained as follows: the theoretical results are presented for the single atom response whereas experimentally the medium response is measured. The phase matching of the HHG in the medium depends, in particular, on the harmonic phase variation with the laser intensity. The slope of this variation depends on the laser ellipticity. The change of the slope can deteriorate phase matching for large ellipticities [10], so the medium

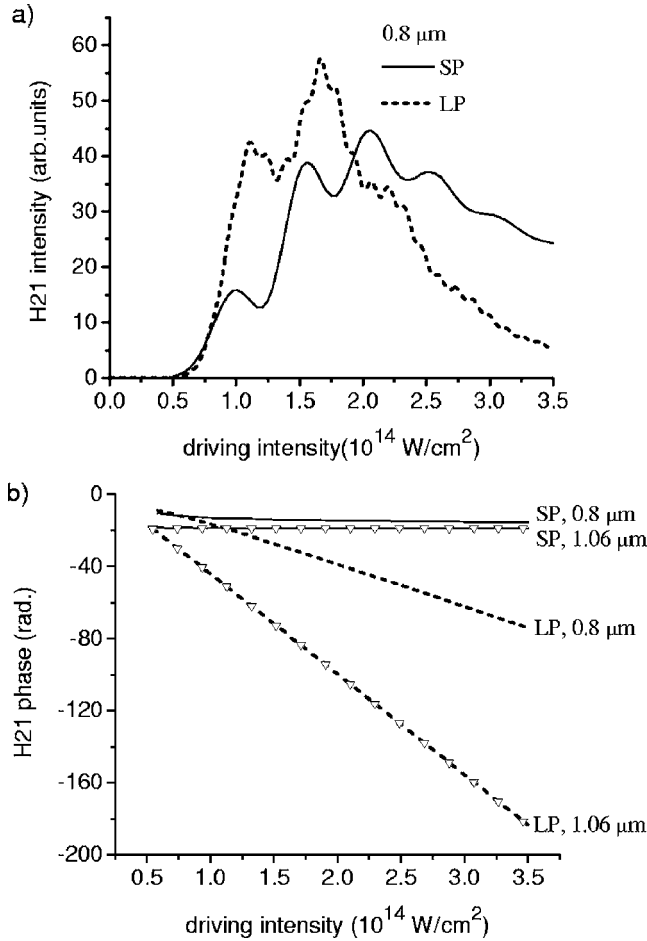


FIG. 5. The same as in Fig. 4, for the 21st harmonic.

response can decrease faster with ellipticity than the single atom response does. The other probable reason is that in our calculations we consider summarized intensities of  $x$  and  $y$  component of the harmonic field, whereas experimentally the measurement efficiency can be different for the two components. We can see that the threshold ellipticities for the shorter and the longer quantum paths are close to each other. The reason is that the greater transverse size of the wave packet having the longer travel time compensates for the higher  $y$  displacement for the longer quantum path [37]. Usually the threshold ellipticity for the shorter path is slightly lower.

In Fig. 7 we show harmonic  $x$  and  $y$  components intensities and phases as functions of the driving ellipticity squared. We can see that the dependence of the  $x$  component's intensity on the driving ellipticity is almost Gaussian, and the harmonic phases depend almost linearly on the square of the ellipticity. Calculating these dependences for other harmonics we find that this dependence is very typical. The deviation from this law for the phases is found only for harmonics whose  $y$  component passes through zero for nonzero driving ellipticities: near these ellipticities the phase is a non-linear function of the driving ellipticity squared.

The linear dependence of the phase of the  $q$ th harmonic on the driving intensity in the plateau region, and on the square of the driving ellipticity can be presented as

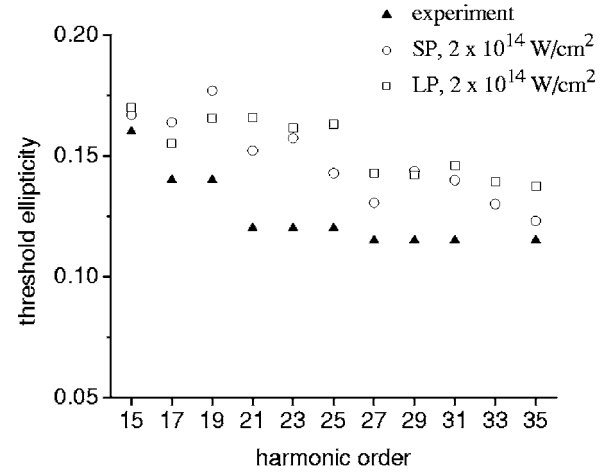


FIG. 6. Threshold ellipticity (i.e., the driving ellipticity for which the harmonic signal is twice as low as that for the linearly-polarized driving field) measured experimentally in Ref. [22] and calculated theoretically. The theory predicts correctly the tendency, but the absolute values somewhat differ. The possible explanations are discussed in the text.

$$\varphi_q^{SP,LP;x,y} \approx -(\alpha_q^{SP,LP} + \mu_q^{SP,LP} \varepsilon^2) \frac{U}{\hbar \omega_0} + \delta_q^{SP,LP;x,y}, \quad (54)$$

where the terms  $\delta_q^{SP,LP;x,y}$  describe the dephasing of different harmonics. For the lower plateau harmonics  $\alpha_q^{LP,x} \approx 2\pi$  (in agreement with the results of Ref. [14]),  $\alpha_q^{SP} \ll \alpha_q^{LP}$ . The coefficients  $\alpha$  depend smoothly on the harmonic number, and the driving ellipticity and frequency. In contrast, the coefficients  $\mu$  are pretty sensitive to these parameters. Note that a similar equation was obtained in Ref. [37]; however, in that paper we considered only single driving frequency and thus did not discuss the behavior of the phase for different driving frequencies.

Finally, in Fig. 8 we show the harmonic ellipticity and the angle of rotation (also called offset angle) of the major axis of the harmonic polarization ellipse, both as functions of the driving ellipticity. These parameters are calculated using intensities and phases of the  $x$  and  $y$  components of the harmonic field utilizing the Stokes parameters as described in [55]; the application of the method for harmonic fields is presented in [10]. The positive harmonic ellipticity means that the harmonic electric field vector turns in the same direction as that of the driving field. The positive rotation angle corresponds to the rotation of the axes of the harmonic polarization ellipse in the direction in which the driving electric field vector turns; the rotation angle is measured with respect to the  $x$  axis. We can see that the behavior of the harmonic ellipticity can be nonmonotonous. However, separation of the shorter and the longer path contributions makes this behavior more straightforward: the dependence of the total (i.e., including all quantum paths) single atom response on the driving ellipticity calculated in Refs. [10,11] is much more complicated because it is strongly affected by the interference of the contributions from different quantum paths.

The behavior of the harmonic ellipticity for the neighbor harmonics can be qualitatively different: in Fig. 8(a) we can

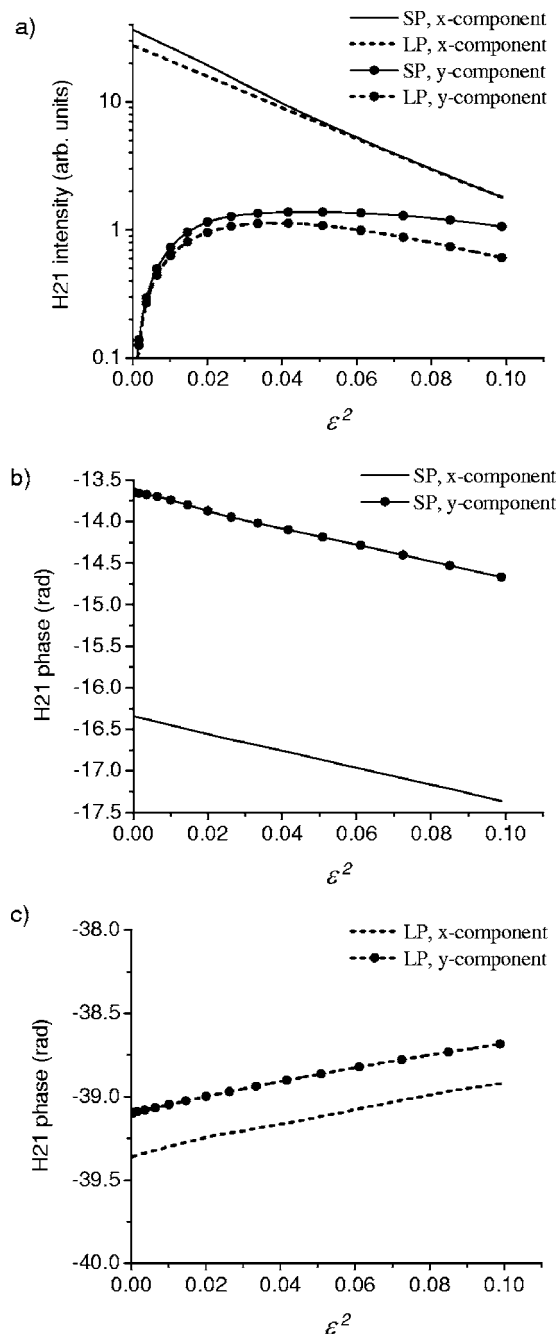


FIG. 7. Intensities (a) and phases (b), (c) of the components of the 21st harmonic as functions of the driving ellipticity squared. The contributions of the shorter and the longer quantum paths are shown with solid and dashed lines, respectively; lines with symbols show the y-component, and the lines without them show the x-component of the harmonic. The driving intensity is  $2 \times 10^{14} \text{ W/cm}^2$ . An approximately linear dependence of the phase of each component on the square of the driving ellipticity can be seen.

see that the ellipticity of the 21st harmonic is always positive, whereas the ellipticity of the LP component of the 19th harmonic for high driving ellipticities is negative. In contrast, the rotation angle depends on the driving ellipticity almost linearly for both harmonics. The behavior presented in Fig. 8(b) is typical: the SP harmonic rotation angle is

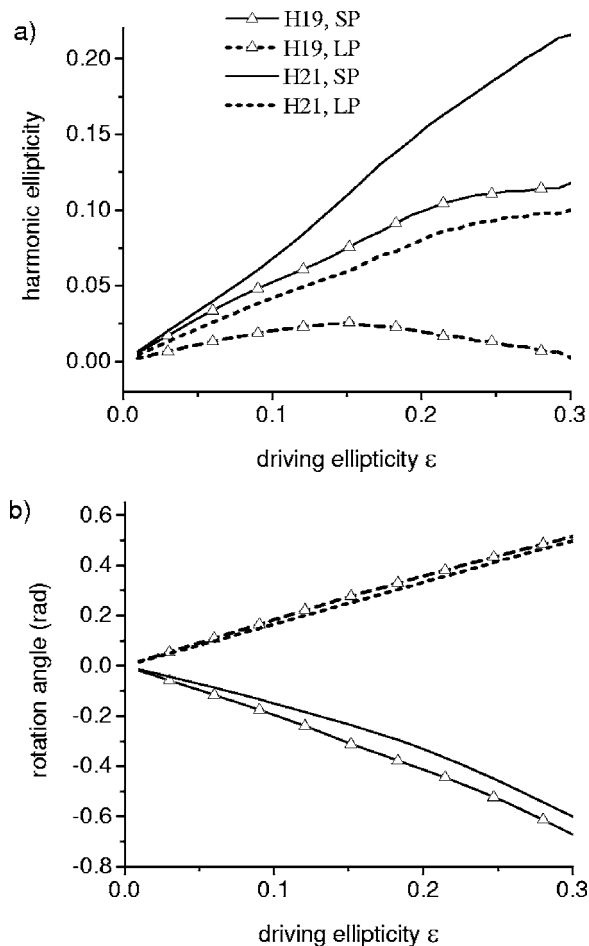


FIG. 8. Harmonic ellipticity (a) and rotation angle of the polarization ellipse (b) for the 19th (lines with symbols) and 21st (lines without symbols) harmonics as functions of the driving ellipticity. One can see that the behaviors of the ellipticity for the neighbor harmonics are essentially different, whereas the behaviors of the rotation angles are close. Rotation angles depend approximately linearly on the driving ellipticity and have different signs for the contributions of the shorter and the longer quantum paths.

negative, the LP one is positive. This can be explained considering the geometry of the trajectories of the electron generating the harmonic (Fig. 9). For the LP component the quasiclassical trajectory starts in the origin and comes back to the origin; the major axis of the harmonic polarization ellipse is approximately collinear with the velocity of the returning electron and thus it is rotated in the positive (clockwise) direction. For the SP component a family of trajectories [corresponding to various  $y$  projections of the initial velocity, see discussion after Eqs. (38)–(40)] should be taken into account; however, all of these trajectories provide negative  $y$  projection of the final velocity and thus the rotation angle is negative. These considerations also explain the linear dependence of the rotation angle on the driving ellipticity: the total picture scales in the  $y$  direction with the  $y$  projection of the driving field which is approximately proportional to the ellipticity (for the small ellipticities considered here). The linear dependence of the rotation angle on the driving ellipticity in Fig. 8(b) is especially obvious for

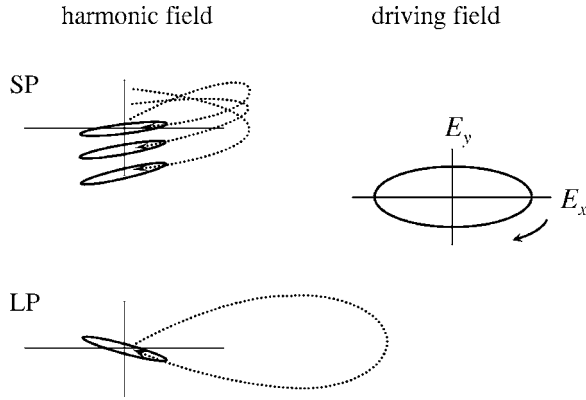


FIG. 9. Qualitative explanation of the behavior of the harmonic rotation angle. The driving field is elliptically polarized and the turning direction of the driving electric field vector is shown with an arrow and denoted below as the positive direction. Dotted curves show classical trajectories of the electron corresponding to the generation of the SP and the LP components of a harmonic. Orientations of the harmonic polarization ellipse are also presented. The orientation is controlled by the direction of the velocity of the returning electron: the major axis is approximately collinear with it. Thus the ellipse is rotated in the positive direction for the LP component and in the negative direction for the SP component. The whole picture approximately scales in  $y$  direction with the driving ellipticity, providing the linear dependence of the rotation angle on it. See text for detailed discussion.

the LP component. Some deviation from the linear law for the SP component originates from the poor applicability of the quasiclassical consideration of the motion in the  $y$  direction for this component discussed above.

The slope of the rotation angle as a function of the driving ellipticity in Fig. 8(b) is smaller for the higher harmonic. For the cut-off harmonics we find rotation angles close to zero. Thus our results are much more close to the predictions of the effective-dipole model, than those of the zero-range model (see Ref. [11] and references therein; in particular, the rotation angles predicted by the two models are compared in Fig. 6(b) in [11]).

The linear dependence of the rotation angle on the driving ellipticity was shown experimentally by Weihe *et al.* [56,57]. However, a detailed comparison of the theoretically predicted properties of the harmonic polarization with an experiment must include propagation calculation: as we have shown above the polarization properties of the single atom response for the SP and LP contributions are essentially different, and their impact on the experimentally measured medium response depend on the propagation features. For the theory suggested in [10] such comparison was done in [58]. The medium response calculation using our theory was done in [22,37–40] with the method described in [59], however, without focusing on the polarization properties. Studying the polarization properties of the medium response will be the subject of our future work.

## V. DISCUSSION

In this section we discuss some features of the theory and the above presented results.

As we have already noted, the dependence of the harmonic phase on the driving intensity is very sensitive to the driving frequency [the slope of the dependence is inversely proportional to the frequency cube, see Figs. 4(b) and 5(b) and Eq. (50)]. So this dependence should be especially important for the HHG with several micron driving field [31–33]. In particular, in such experiments this dependence can have a dramatic effect on the HHG phase matching and cause an essential broadening of the harmonic line.

In the previous section we stressed that the behavior of the SP and LP contributions taken separately is more straightforward than that of the total harmonic response. There is another (more technical, however, practically important) advantage of this separation. The total harmonic response oscillates rapidly as a function of the driving field parameters due to the interference of the SP and LP contributions. Therefore calculating the medium response using the total single-atom harmonic response implies numerical integration of rapidly oscillating functions. This requires more computations than the separate integration of the two contributions does because both contributions are smooth functions of the driving field parameters. Moreover, for the case of the linearly polarized Gaussian driving beam separating the contributions allows approximate analytical study of the HHG phase matching in the medium [60].

In this paper we present the results calculated for Argon atom. Evidently, our approach is applicable for other atoms as well. In this case one should use the ionization potential  $I$  of the desired atom and the corresponding ionization rate  $w(E)$  (calculated numerically using a model potential, or analytically, e.g., using results of Ref. [61]). Besides, we used the nonperturbed ground state wave function given by Eq. (8) as a bound state in our theory. A further development of the theory can include the ground state modification by the laser field, for example, taking into account the Stark shift of the ground state energy as it was done in Ref. [19]. Moreover, an excited ground state can be considered to investigate HHG with a preexcited atom, which was recently done with numerical simulation in Ref. [62].

In our approach we neglect the magnetic component of the field. However the action of this component can be taken into account via modification of the electronic trajectory and the wave packet phase due to the Lorentz force.

## VI. CONCLUSIONS

We present the HHG theory based on strong field approximation and quasiclassical description of the free electron motion along the major axis of the driving field polarization ellipse.

The distinct features of the developed theory are following. The electron motion in the transverse (to the major axis) plane is considered quantum mechanically. We find a condition under which the latter motion can also be described quasiclassically, thus the free electron motion can be reduced to a quantum orbit in the polarization plane of the driving field. The ionization rate calculated numerically via TDSE solution for the model atomic potential is used. We take into account the Coulomb attraction of the wave packet after the



ionization (with the parameter  $\delta$  that is optimized to fit the numerical results), and the Coulomb modification of the returning wave packet.

These features allowed us to achieve a good agreement of the theoretical results with the numerical TDSE solution for linearly-polarized driving laser pulses of various intensities. In particular, our theory predicts correctly the ratio of the two quantum path contributions. For the case of elliptically-polarized field the predictions of our theory agree with the experimentally measured threshold ellipticities for different harmonics.

Being based on the quasiclassical description of the electronic motion (at least in one direction), our approach is, strictly speaking, applicable in the tunneling limit. However, the comparison with the numerical results shows that the theory is valid even for the Keldysh parameter  $\gamma \sim 1$ . Our theory is applicable if the driving ellipticity is not too high, namely, for  $\varepsilon < \sqrt{2}\gamma$ ; the upper limit of this validity range essentially exceeds the threshold ellipticity.

Our theory allows calculating separately the contributions of the different quantum paths to a harmonic field; in this paper we study the quantum paths with the travel time less than one optical cycle. We show the properties of these con-

tributions as functions of the intensity and ellipticity of the driving field. Presented separately, these contributions demonstrate a simpler behavior than that of the total harmonic atomic response investigated in earlier studies. In particular, the phases depend linearly on the driving intensity and on the square of the driving ellipticity, and the slope is inversely proportional to the driving frequency cube. The rotation angles of the polarization ellipses depend linearly on the driving ellipticity, and the slope has different sign for the two contributions. We explain this behavior linking the orientation of the harmonic polarization ellipse to the quantum orbit geometry.

## ACKNOWLEDGMENTS

The author acknowledges fruitful discussions with E. Constant, E. Mevel, E. Cormier, V. Platonenko, B. Carre, W. Becker, A. L'Huillier, S. Goreslavsky, M. Ryabikin, and N. Shubin. This study was supported by the French Ministry of Education, Presidium of the Russian Academy of Sciences (Program "Femtosecond Optics and Novel Optical Materials"), the Russian Science Support Foundation and the "Dynasty" Foundation.

- 
- [1] P. M. Paul *et al.*, *Science* **292**, 1689 (2001).
  - [2] P. B. Corkum, *Phys. Rev. Lett.* **71**, 1994 (1993).
  - [3] K. J. Schafer, B. Yang, L. F. DiMauro, and K. C. Kulander, *Phys. Rev. Lett.* **70**, 1599 (1993).
  - [4] K. C. Kulander, K. J. Schafer, and J. L. Krause, in *Super-Intense Laser-Atom Physics*, Vol. 316 of NATO Advanced Studies Institute, Series B: Physics (Plenum, New York, 1993), p. 95.
  - [5] A. L'Huillier, M. Lewenstein, P. Salieres, P. Balcou, M. Y. Ivanov, J. Larsson, and C. G. Wahlstrom, *Phys. Rev. A* **48**, R3433 (1993).
  - [6] M. Lewenstein, P. Balcou, M. Y. Ivanov, A. L'Huillier, and P. B. Corkum, *Phys. Rev. A* **49**, 2117 (1994).
  - [7] W. Becker, S. Long, and J. K. McIver, *Phys. Rev. A* **50**, 1540 (1994).
  - [8] V. T. Platonenko and V. V. Strelkov, *Quantum Electron.* **25**, 564 (1998).
  - [9] L. V. Keldysh, *Sov. Phys. JETP* **20**, 1307 (1964); F. H. M. Faisal, *J. Phys. B* **6**, L89 (1973); H. R. Reiss, *Phys. Rev. A* **22**, 1786 (1980).
  - [10] Ph. Antoine, A. L'Huillier, M. Lewenstein, P. Salieres, and B. Carre, *Phys. Rev. A* **53**, 1725 (1996).
  - [11] W. Becker, A. Lohr, M. Kleber, and M. Lewenstein, *Phys. Rev. A* **56**, 645 (1997).
  - [12] M. Lewenstein, P. Salieres, and A. L'Huillier, *Phys. Rev. A* **52**, 4747 (1995).
  - [13] G. G. Paulus, F. Grasbon, A. Dreischuh, H. Walther, R. Koppold, and W. Becker, *Phys. Rev. Lett.* **84**, 3791 (2000).
  - [14] P. Salieres *et al.*, *Science* **292**, 902 (2001).
  - [15] D. B. Milošević, D. Bauer, and W. Becker, *J. Mod. Opt.* **53**, 125 (2006).
  - [16] W. Becker *et al.*, *Adv. At., Mol., Opt. Phys.* **48**, 35 (2002).
  - [17] D. Bauer, D. B. Milošević, and W. Becker, *J. Mod. Opt.* **53**, 135 (2006).
  - [18] D. Bauer, *Phys. Rev. Lett.* **94**, 113001 (2005).
  - [19] M. Yu. Ivanov, Th. Brabec, and N. Burnett, *Phys. Rev. A* **54**, 742 (1996).
  - [20] V. T. Platonenko, *Quantum Electron.* **31**, 55 (2001).
  - [21] P. B. Corkum, N. H. Burnett, and M. Yu. Ivanov, *Opt. Lett.* **19**, 1870 (1994).
  - [22] I. Sola *et al.*, *Nat. Phys.* **2**, 281 (2006).
  - [23] L. D. Landau and E. M. Lifshitz, *Quantum Mechanics*, Sec. 136 (Pergamon Press, Oxford, 1977).
  - [24] S. Basile, F. Trombetta, G. Ferrante, R. Burlon, and C. Leone, *Phys. Rev. A* **37**, 1050 (1988).
  - [25] J. Z. Kaminski, A. Jaron, and F. Ehlotzky, *Phys. Rev. A* **53**, 1756 (1996).
  - [26] S. P. Goreslavsky and S. V. Popruzhenko, *Laser Phys.* **8**, 1 (1998).
  - [27] S. P. Goreslavsky and S. V. Popruzhenko, *J. Exp. Theor. Phys.* **90**, 778 (2000) [translated from *Zh. Eksp. Teor. Fiz.* **117**, 895 (2000)].
  - [28] A. M. Perelomov, V. S. Popov, and M. V. Terentev, *Zh. Eksp. Teor. Fiz.* **50**, 1393 (1966) [*Sov. Phys. JETP* **23**, 924 (1966)].
  - [29] G. G. Paulus, W. Becker, and H. Walther, *Phys. Rev. A* **52**, 4043 (1995).
  - [30] V. V. Strelkov *et al.*, *J. Phys. B* **39**, 577 (2006).
  - [31] B. Sheehy, J. D. D. Martin, L. F. DiMauro, P. Agostini, K. J. Schafer, M. B. Gaarde, and K. C. Kulander, *Phys. Rev. Lett.* **83**, 5270 (1999).
  - [32] B. Shan and Z. Chang, *Phys. Rev. A* **65**, 011804(R) (2002).
  - [33] A. Gordon and F. Kartner, *Opt. Express* **13**, 2941 (2005).
  - [34] S. P. Goreslavski, G. G. Paulus, S. V. Popruzhenko, and N. I. Shvetsov-Shilovski, *Phys. Rev. Lett.* **93**, 233002 (2004).

- [35] V. V. Strelkov, V. T. Platonenko, and A. Becker, *Phys. Rev. A* **71**, 053808 (2005).
- [36] D. Bauer and P. Mulser, *Phys. Rev. A* **59**, 569 (1999).
- [37] V. Strelkov *et al.*, *Appl. Phys. B: Lasers Opt.* **78**, 879 (2004).
- [38] V. Strelkov *et al.*, *Laser Phys.* **15**, 871 (2005).
- [39] V. Strelkov *et al.*, *J. Phys. B* **38**, L161 (2005).
- [40] I. Sola *et al.*, *Phys. Rev. A* (to be published).
- [41] E. Cormier and P. Lambropoulos, *J. Phys. B* **30**, 77 (1997).
- [42] H. G. Muller, *Phys. Rev. A* **60**, 1341 (1999).
- [43] M. Gavrilu, *J. Phys. B* **35**, R147 (2002).
- [44] M. Hentschel *et al.*, *Nature (London)* **414**, 509 (2001).
- [45] Y. Mairesse *et al.*, *Science* **302**, 1540 (2003).
- [46] P. Tzallas *et al.*, *Nature (London)* **426**, 267 (2003).
- [47] P. Antoine, A. L'Huillier, and M. Lewenstein, *Phys. Rev. Lett.* **77**, 1234 (1996).
- [48] V. T. Platonenko and V. V. Strelkov, *Quantum Electron.* **24**, 779 (1997).
- [49] R. Kopold, D. B. Milosevic, and W. Becker, *Phys. Rev. Lett.* **84**, 3831 (2000).
- [50] M. B. Gaarde, F. Salin, E. Constant, P. Balcou, K. J. Schafer, K. C. Kulander, and A. L'Huillier, *Phys. Rev. A* **59**, 1367 (1999).
- [51] P. Balcou *et al.*, *J. Phys. B* **32**, 2973 (1999).
- [52] M. B. Gaarde and K. J. Schafer, *Phys. Rev. A* **65**, 031406(R) (2002).
- [53] K. S. Budil, P. Salieres, A. L'Huillier, T. Ditmire, and M. D. Perry, *Phys. Rev. A* **48**, R3437 (1993).
- [54] P. Dietrich, N. H. Burnett, M. Ivanov, and P. B. Corkum, *Phys. Rev. A* **50**, R3585 (1994).
- [55] M. Born and E. Wolf, *Principles of Optics* (Pergamon, New York, 1964).
- [56] F. A. Weihe, S. K. Dutta, G. Korn, D. Du, P. H. Bucksbaum, and P. L. Shkolnikov, *Phys. Rev. A* **51**, R3433 (1995).
- [57] F. A. Weihe *et al.*, *J. Opt. Soc. Am. B* **13**, 157 (1996).
- [58] Ph. Antoine, B. Carre, A. L'Huillier, and M. Lewenstein, *Phys. Rev. A* **55**, 1314 (1997).
- [59] V. Platonenko, V. Strelkov, and G. Ferrante, *J. Opt. Soc. Am. B* **19**, 1611 (2002).
- [60] S. Batebi and V. T. Platonenko, *Quantum Electron.* **34**, 71 (2004).
- [61] G. L. Yudin and M. Yu. Ivanov, *Phys. Rev. A* **64**, 013409 (2001).
- [62] M. Yu. Emelin *et al.*, *Europhys. Lett.* **69**, 913 (2005).